Earth and Planetary Science Letters 432 (2015) 152–165

Contents lists available at ScienceDirect

Earth and Planetary Science Letters

www.elsevier.com/locate/epsl

A process-based model for non-equilibrium clumped isotope effects in carbonates

J.M. Watkins [a,*], J.D. Hunt [b]

[a] Dept. of Geological Sciences, University of Oregon, United States
[b] Ramboll Environ, United States

ARTICLE INFO

Article history:
Received 30 May 2015
Received in revised form 26 August 2015
Accepted 28 September 2015
Available online xxxx
Editor: H. Stoll

Keywords:
clumped isotopes
oxygen isotopes
equilibrium
kinetic
calcite
paleothermometry

ABSTRACT

The equilibrium clumped isotope composition of carbonate minerals is independent of the composition of the aqueous solution. However, many carbonate minerals grow at rates that place them in a non-equilibrium regime with respect to carbon and oxygen isotopes with unknown consequences for clumped isotopes. We develop a process-based model that allows one to calculate the oxygen, carbon, and clumped isotope composition of calcite as a function of temperature, crystal growth rate, and solution pH. In the model, carbon and oxygen isotope fractionation occurs through the mass-dependent attachment/detachment kinetics of the isotopologues of HCO_3^- and CO_3^{2-} to and from the calcite surface, which in turn, influence the clumped isotope composition of calcite. At experimental and biogenic growth rates, the mineral is expected to inherit a clumped isotopic composition that is similar to that of the DIC pool, which helps to explain (1) why different organisms share the same clumped isotope versus temperature calibration curves, (2) why many inorganic calibration curves are slightly different from one another, and (3) why foraminifera, coccoliths, and deep sea corals can have near-equilibrium clumped isotope compositions but far-from-equilibrium carbon and oxygen isotope compositions. Some aspects of the model can be generalized to other mineral systems and should serve as a useful reference in future efforts to quantify kinetic clumped isotope effects.

Published by Elsevier B.V.

1. Introduction

Clumped isotope geochemistry, or the study of bond ordering in molecules, is at the frontier of efforts to use temperature proxies for reconstructing ocean chemistry (Came et al., 2007), estimating the uplift rate of mountains (Ghosh et al., 2006b), studying diagenetic processes (Dennis and Schrag, 2010), sourcing methane (Stolper et al., 2014, 2015; Wang et al., 2015), identifying signatures of biology in the atmosphere (Yeung et al., 2015) and even investigating the thermal physiology of dinosaurs (Eagle et al., 2011). The most widely-used clumped isotope thermometer is based on the homogeneous reaction (Ghosh et al., 2006a):

$$\underbrace{^{13}C^{16}O_3^{2-}}_{\text{mass 61}} + \underbrace{^{12}C^{18}O^{16}O_2^{2-}}_{\text{mass 62}} \rightleftharpoons \underbrace{^{13}C^{18}O^{16}O_2^{2-}}_{\text{mass 63}} + \underbrace{^{12}C^{16}O_3^{2-}}_{\text{mass 60}}, \quad (1)$$

which describes the extent to which the rare isotopes ^{13}C and ^{18}O are bound together as 'clumps' among the carbonate molecules. The equilibrium constant for this reaction, which can be applied to either dissolved carbonate molecules or carbonate molecules in minerals such as calcite, has a well-defined temperature-dependence based on equilibrium thermodynamics (Wang et al., 2004; Schauble et al., 2006) and is measured by expressing the proportion of mass 63 isotopologues relative to what one would expect for a stochastic distribution of isotopes among the carbonate isotopologues (Ghosh et al., 2006a).

Because the clumped isotope thermometer is based on equilibrium thermodynamics, it potentially suffers from the same issue as oxygen isotope thermometry: many carbonates that form in nature grow at rates that place them in a non-equilibrium regime (Dietzel et al., 2009). There are clear instances, for example in speleothems and surface corals, where clumped isotope compositions yield significant over- or under-estimates of temperature, representing clear departures from equilibrium (Affek et al., 2008; Daëron et al., 2011; Saenger et al., 2012; Affek, 2012; Eiler et al., 2014). There are other cases, namely in deep-sea corals, where clumped isotope compositions are apparently equilibrated even when there are significant departures from carbon and oxygen isotope equilibrium (Thiagarajan et al., 2011; Eiler et al., 2014). Several ideas have been put forth to explain these observations, but because of the complexity of clumped iso-

* Corresponding author.
E-mail address: watkins4@uoregon.edu (J.M. Watkins).

http://dx.doi.org/10.1016/j.epsl.2015.09.042
0012-821X/Published by Elsevier B.V.

tope systematics relative to oxygen or carbon isotope systematics, the models have remained largely conceptual (Tang et al., 2014; Tripati et al., 2015) or based on analogies to gas phase processes such as Knudsen diffusion and mixing of indestructible molecules (Thiagarajan et al., 2011; Henkes et al., 2013).

In this paper we employ a process-based crystal growth model to investigate the complex interplay between carbon, oxygen, and clumped isotope systematics during carbonate growth under non-equilibrium conditions. The non-equilibrium isotope effects attending carbonate precipitation are quantified by considering the mass-dependent transport of isotopologues of CO_3^{2-} and HCO_3^- to and from the mineral surface. In this framework, the carbon isotope composition is calculated from the ratio of $^{13}C^{16}O^{16}O^{16}O$ (mass 61) to $^{12}C^{16}O^{16}O^{16}O$ (mass 60) ions incorporated into the mineral, and the oxygen isotope composition is calculated from the ratio of $^{12}C^{18}O^{16}O^{16}O$ (mass 62) to $^{12}C^{16}O^{16}O^{16}O$ (mass 60) incorporated into the mineral. Since each dissolved inorganic carbon ($DIC = CO_2(aq) + HCO_3^- + CO_3^{2-}$) species has a different equilibrium carbon, oxygen, and clumped isotopic composition (Zeebe and Wolf-Gladrow, 2001; Beck et al., 2005; Hill et al., 2014), the net carbon and oxygen isotopic composition of calcite depends on the relative proportions of HCO_3^- and CO_3^{2-} participating in calcite growth, the isotopic compositions of dissolved HCO_3^- and CO_3^{2-}, and any isotopic fractionations (equilibrium or kinetic) between calcite and each species that arise during ion transport onto, or away from, the mineral surface. The processes could include aqueous diffusion, isotope exchange reactions in aqueous solution, desolvation, surface diffusion and isotope exchange reactions at or near the aqueous–mineral interface. For clumped isotopes, the $^{13}C^{18}O^{16}O^{16}O$ isotopologue (mass 63) is postulated to follow a mass fractionation law that is mathematically related to the behavior of the mass 62 and mass 61 isotopologues.

2. Notation

2.1. Notation for carbon and oxygen isotopes

The difference in isotope composition between any two chemical species or phases can be expressed in terms of an isotopic fractionation factor (α). The fractionation factors between calcite and DIC (for carbon isotopes) and calcite and water (for oxygen isotopes) are given by:

$$\alpha^{C}_{xtl-DIC} = \frac{\left(\frac{[^{13}C]}{[^{12}C]}\right)_{xtl}}{\left(\frac{[^{13}C]}{[^{12}C]}\right)_{DIC}}, \tag{2}$$

and

$$\alpha^{O}_{xtl-w} = \frac{\left(\frac{[^{18}O]}{[^{16}O]}\right)_{xtl}}{\left(\frac{[^{18}O]}{[^{16}O]}\right)_{w}}, \tag{3}$$

where the subscript 'xtl' refers to calcite and 'w' refers to water. The *equilibrium* isotope compositions for species dissolved in aqueous solution are plotted as curves in Fig. 1. The fractionation factors used to construct these curves are provided in Table 1 along with the appropriate references. Note that the oxygen isotope composition of DIC varies with pH because it represents a weighted average of the isotopic composition of individual species. The carbon isotope composition of DIC is also a weighted average of DIC, but is constant with pH because DIC is the only carbon in the system (there is no carbon in H_2O). Hence, the carbon isotope composition of each dissolved species must vary as a consequence of mass balance (cf. Zeebe and Wolf-Gladrow, 2001).

All model calculations in this paper will be done under the assumption that the system is water buffered such that the equilibrium $^{18}O/^{16}O$ values of the DIC species are controlled solely by temperature and the $^{18}O/^{16}O$ of the water. We also assume an infinite reservoir such that the DIC concentration and $^{13}C/^{12}C$ of DIC are constant in all calculations; i.e., there is no distillation of carbon isotopes or change in pH as the carbonate precipitates.

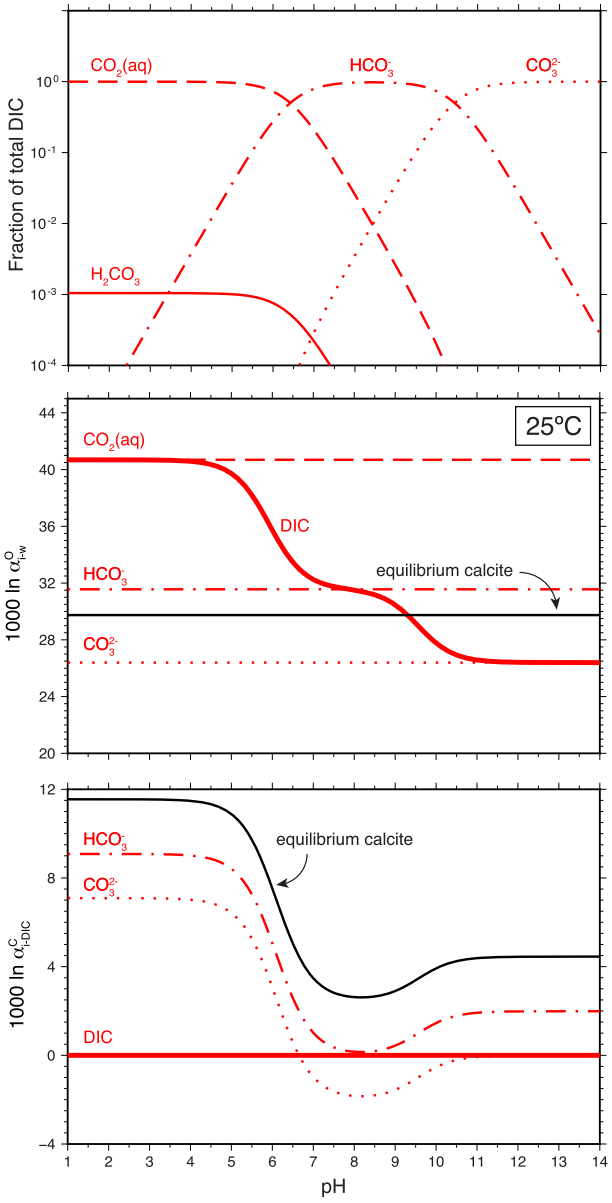

Fig. 1. Equilibrium stable isotope composition of calcite and dissolved inorganic carbon (DIC) species in aqueous solution. *Top*: Distribution of DIC species in aqueous solution as a function of pH. *Middle*: Oxygen isotope compositions expressed relative to water. Since water is by far the predominant oxygen-bearing species in aqueous solution, mass balance dictates that the oxygen isotope composition of DIC vary with pH. *Bottom*: Carbon isotope compositions expressed relative to DIC. Since all of the carbon in aqueous solution is stored in DIC, mass balance dictates that the carbon isotope composition of DIC be constant with pH. Also shown are proposed curves for the equilibrium stable isotope composition of calcite. See Table 2 for the equilibrium fractionation factors used to construct these curves.

2.2. Notation for clumped isotopes

The clumped isotope composition of calcite, denoted Δ^{63}_{xtl}, is given by

$$\Delta^{63}_{xtl} = 1000\left(\frac{r^{63}_{xtl}}{r^{63}_{xtl}*} - 1\right), \tag{4}$$

Table 1
Compilation of equilibrium fractionation factors (α^{eq}_{i-j} unless otherwise noted) for carbon and oxygen isotopes in aqueous solution. These equations are presented graphically in Fig. 1 (note: $\Delta = 1000 \ln \alpha$).

Compounds	Equation	α (25 °C)	References
Carbon isotopes			
$CO_2(g)$ – HCO_3^-	$-9.483/T_K + 1.0239$	0.9921	Mook et al. (1974) as in Mook (1986)
$CO_2(aq)$ – HCO_3^-	$-9.866/T_K + 1.0241$	0.9910	Vogel et al. (1970) as in Mook (1986)
CO_3^{2-} – HCO_3^-	$-0.867/T_K + 1.0025$	0.9996	Turner (1982) as in Mook (1986)
$CO_2(g)$ – calcite	$\Delta = -2.988 \cdot 10^6/T_K^2 + 7.666 \cdot 10^3/T_K - 2.461$	0.9897	Bottinga (1968)
Oxygen isotopes			
$CO_2(g)$ – H_2O	$17.611/T_K + 0.9821$	1.0412	Zeebe (2007)
$CO_2(aq)$ – H_2O	$17.54/T_K + 0.9827$	1.0415	Wang et al. (2013)
HCO_3^- – H_2O	$17.76/T_K + 0.9725$	1.0321	Wang et al. (2013)
CO_3^{2-} – H_2O	$21.72/T_K + 0.9539$	1.0268	Wang et al. (2013)
Calcite – H_2O	$\Delta = 17747/T_K - 29.777$	1.0302	Coplen (2007), Watkins et al. (2013)

Table 2
Descriptions of symbols used to calculate the isotopic composition of non-equilibrium calcite.

Symbol	Description
AR^{60}	Attachment rate of mass 60 isotopologue
DR^{60}	Detachment rate of mass 60 isotopologue
ϕ	HCO_3^-/CO_3^{2-} in solution
R^C_{xtl}	Molar ratio of $^{13}C/^{12}C$ in the crystal
R^O_{xtl}	Molar ratio of $^{18}O/^{16}O$ in the crystal
r^{61}_{xtl}	Molar ratio of mass 61 to mass 60 isotopologues in the crystal
$r^{eq,61}_{xtl}$	Equilibrium molar ratio of mass 61 to mass 60 isotopologues in the crystal
r^{62}_{xtl}	Molar ratio of mass 62 to mass 60 isotopologues in the crystal
r^{63}_{xtl}	Molar ratio of mass 63 to mass 60 isotopologues in the crystal
$r^{63}_{xtl^*}$	Stochastic molar ratio of mass 63 to mass 60 isotopologues in the crystal
$\alpha^{eq,C}_{xtl-B_1}$	Equilibrium carbon isotope fractionation factor between calcite and dissolved CO_3^{2-}
$\alpha^{eq,C}_{xtl-B_2}$	Equilibrium carbon isotope fractionation factor between calcite and dissolved HCO_3^-
$\alpha^{eq,O}_{xtl-B_1}$	Equilibrium oxygen isotope fractionation factor between calcite and dissolved CO_3^{2-}
$\alpha^{eq,O}_{xtl-B_2}$	Equilibrium oxygen isotope fractionation factor between calcite and dissolved HCO_3^-
$\alpha^{eq,63}_{xtl-B_1}$	Equilibrium clumped isotope fractionation factor between calcite and dissolved CO_3^{2-}
$\alpha^{eq,63}_{xtl-B_2}$	Equilibrium clumped isotope fractionation factor between calcite and dissolved HCO_3^-
$\alpha^{eq,C}_{B_2-B_1}$	Equilibrium carbon isotope fractionation factor between dissolved HCO_3^- and CO_3^{2-}
$\alpha^{eq,O}_{B_2-B_1}$	Equilibrium oxygen isotope fractionation factor between dissolved HCO_3^- and CO_3^{2-}
$\alpha^{f,C}_{xtl-B_1}$	Kinetic carbon isotope fractionation factor between calcite and dissolved CO_3^{2-}
$\alpha^{f,C}_{xtl-B_2}$	Kinetic carbon isotope fractionation factor between calcite and dissolved HCO_3^-
$\alpha^{f,O}_{xtl-B_1}$	Kinetic oxygen isotope fractionation factor between calcite and dissolved CO_3^{2-}
$\alpha^{f,O}_{xtl-B_2}$	Kinetic oxygen isotope fractionation factor between calcite and dissolved HCO_3^-
$\alpha^{f,63}_{xtl-B_1}$	Kinetic clumped isotope fractionation factor between calcite and dissolved CO_3^{2-}
$\alpha^{f,63}_{xtl-B_2}$	Kinetic clumped isotope fractionation factor between calcite and dissolved HCO_3^-
ϵ_{B_1}	Describes the extent of isotopic scrambling (negative values) or unscrambling (positive values) of CO_3^{2-} during transport from the solution to the crystal
ϵ_{B_2}	Describes the extent of isotopic scrambling (negative values) or unscrambling (positive values) of HCO_3^- during transport from the solution to the crystal

where

$$r^{63}_{xtl} = \frac{^{13}C^{18}O^{16}O^{16}O}{^{12}C^{16}O^{16}O^{16}O}, \quad (5)$$

and the asterisk in Eq. (4) denotes the stochastic ratio, which can be calculated from knowledge of the oxygen and carbon isotope compositions (Eiler and Schauble, 2004). Note that clumped isotope compositions are commonly expressed as Δ^{47} because the measurement involves ^{13}C–^{18}O bond ordering in $CO_2(g)$ released upon acid digestion of carbonates. Conversion of Δ^{63} to Δ^{47} is accomplished via an acid digestion fractionation factor (AFF):

$$\Delta^{47} = \Delta^{63} + \text{AFF}, \quad (6)$$

where the AFF depends on the temperature of acid digestion (Defliese et al., 2015), the sample size (Wacker et al., 2013), and perhaps also the clumped isotope composition of the carbonate mineral itself (Guo et al., 2009). These details are important to consider when comparing model results to measurements on natural samples.

2.3. Isotope versus isotopologue ratios

If we consider that only the singly-substituted ^{18}O isotopologue contributes to the oxygen isotope composition of calcite, we have the following relationships between isotope ratios (R) and isotopologue ratios (r):

$$R^{O}_{xtl} = \left(\frac{[^{18}O]}{[^{16}O]}\right)_{xtl} \approx \frac{1}{3} r^{62}_{xtl} = \frac{1}{3}\frac{Ca^{12}C^{18}O^{16}O^{16}O}{Ca^{12}C^{16}O^{16}O^{16}O}, \quad (7)$$

and

$$R^{C}_{xtl} = \left(\frac{[^{13}C]}{[^{12}C]}\right)_{xtl} \approx r^{61}_{xtl} = \frac{Ca^{13}C^{16}O^{16}O^{16}O}{Ca^{12}C^{16}O^{16}O^{16}O}. \quad (8)$$

The factor of 1/3 for oxygen isotopes comes from the fact that there are three oxygen atoms in the CO_3^{2-} molecule, and the approximate signs come from the recognition that the singly-substituted isotopologues are not the only, but by far the most abundant, ^{18}O- or ^{13}C-bearing carbonate molecules (Usdowski and Hoefs, 1993; see Appendix in Watkins et al., 2014 for more details).

For the dissolved species in solution, we use the shorthand notation $B_1 = CO_3^{2-}$ and $B_2 = HCO_3^-$ and write

$$R^{O}_{B_1} = \left(\frac{[^{18}O]}{[^{16}O]}\right)_{B_1} \approx \frac{1}{3} r^{62}_{B_1} = \frac{1}{3}\frac{^{12}C^{18}O^{16}O^{16}O}{^{12}C^{16}O^{16}O^{16}O}, \quad (9)$$

$$R^{C}_{B_1} = \left(\frac{[^{13}C]}{[^{12}C]}\right)_{B_1} \approx r^{61}_{B_1} = \frac{^{13}C^{16}O^{16}O^{16}O}{^{12}C^{16}O^{16}O^{16}O}, \quad (10)$$

$$R^{O}_{B_2} = \left(\frac{[^{18}O]}{[^{16}O]}\right)_{B_2} \approx \frac{1}{3} r^{62}_{B_2} = \frac{1}{3}\frac{H^{12}C^{18}O^{16}O^{16}O}{H^{12}C^{16}O^{16}O^{16}O}, \quad (11)$$

and

$$R^{C}_{B_2} = \left(\frac{[^{13}C]}{[^{12}C]}\right)_{B_2} \approx r^{61}_{B_2} = \frac{H^{13}C^{16}O^{16}O^{16}O}{H^{12}C^{16}O^{16}O^{16}O}. \quad (12)$$

Note that here, and throughout the paper, we ignore the contribution of hydrogen to the mass of HCO_3^- isotopologues such that mass 63 refers to the doubly-substituted isotopologue of HCO_3^- as well as CO_3^{2-}.

3. Ion-by-ion model for carbon and oxygen isotopes

Kinetic isotope effects in carbonates can arise from incomplete carbon and oxygen isotope exchange among DIC species or during transfer of HCO_3^- and CO_3^{2-} ions to the mineral surface and into the mineral lattice. In the simplest scenario, HCO_3^- and CO_3^{2-} exchange kinetics in the aqueous solution are fast enough such that the isotopic compositions of HCO_3^- and CO_3^{2-} are the known equilibrium values (Beck et al., 2005; Zeebe, 2007; Wang et al., 2013). The picture is considerably more complicated when the DIC species are not isotopically equilibrated because, at any given instant, the isotopic compositions of HCO_3^- and CO_3^{2-} are poorly constrained due to limited knowledge of the isotope exchange kinetics and pathways associated with (de-)hydration and (de-)hydroxylation of dissolved CO_2 (Guo, 2009). It is therefore constructive to focus on the case where the isotopic composition of HCO_3^- and CO_3^{2-} are known and constant (i.e., equilibrated) and then discuss the consequences of an unequilibrated DIC pool.

Our starting point is a model for a cubic crystal (an approximation to the calcite rhombohedron) where the attachment and detachment fluxes (moles m^{-2} s^{-1}) of calcium and (bi-)carbonate ions to and from the mineral surface are given by Wolthers et al. (2012):

$$J^{ion}_{attach} = \frac{\rho_c (AR^{ion}) a^2 d}{y_0} \quad (13)$$

and

$$J^{ion}_{detach} = \frac{\rho_c (DR^{ion}) a^2 d}{y_0}, \quad (14)$$

where ρ_c is the steady-state kink site density (dimensionless), AR and DR are attachment rates and detachment rates (s^{-1}) of each ion, $a = 3.199 \times 10^{-10}$ m is the closest spacing between adjacent Ca^{2+} and CO_3^{2-} sites on the calcite surface, $d = 27\,100$ moles m^{-3} is the molar density of calcite and y_0 (m) is the step spacing. The attachment and detachment rates are calculated from the model of Wolthers et al. (2012) and depend on factors such as temperature, pH, salinity, and the calcium:carbonate ratio of the solution (see next section). The net flux of an individual ion is given by the difference

$$J^{ion}_{net} = J^{ion}_{attach} - J^{ion}_{detach}, \quad (15)$$

and the net growth or dissolution rate of the crystal (R_c) is given by

$$R_c = J^{Ca^{2+}}_{net} = J^{B_1}_{net} + J^{B_2}_{net}. \quad (16)$$

3.1. Expressions for the carbon and oxygen isotope composition of non-equilibrium calcite

In the ion-by-ion growth model for oxygen isotopes derived in our previous work (Watkins et al., 2014), the difference in oxygen isotope composition between calcite and water is related to the rates of isotopologue attachment to (AR^i; i is isotopologue mass), and detachment from (DR^i), the mineral surface, as well as the relative contribution of each DIC species to the overall kinetic fractionation:

$$\alpha^{O}_{xtl-w} = \frac{\alpha^{eq,O}_{xtl-w} AR^{60}}{\alpha^{eq,O}_{xtl-w}\left(AR^{60} - DR^{60}\right)\eta + DR^{60}}, \quad (17a)$$

where

$$\eta = \frac{1+\phi}{\alpha^{f,O}_{xtl-B_1}\alpha^{eq,O}_{B_1-w} + \phi\alpha^{f,O}_{xtl-B_2}\alpha^{eq,O}_{B_2-w}} \quad (17b)$$

and ϕ is the ratio of bicarbonate to carbonate dissolved in solution. The α's are the calcite–water fractionation factors in the slow-growth limit ($\alpha^{eq,O}_{xtl-w}$) and fast-growth limit ($\alpha^{f,O}_{xtl-w}$), as discussed further below. These expressions are identical to Eqs. 18a and 18b in Watkins et al. (2014). The attachment and detachment rates (s^{-1}) of the major isotopologues are given by Wolthers et al. (2012):

$$AR^{60} = k_{B_1^{60}}\left[B_1^{60}\right] P_A + k_{B_2^{60}}\left[B_2^{60}\right] P_A, \quad (18)$$

and

$$DR^{60} = \nu^{60}_{B_1} P^{60}_{B_1} + \nu^{60}_{B_2} P^{60}_{B_2}, \quad (19)$$

where the k's (M^{-1} s^{-1}) and ν's (s^{-1}) are mass-dependent attachment and detachment frequencies and the P's are probabilities of a kink site being occupied by a bicarbonate, carbonate, or calcium ion on the crystal surface. All of the values in Eqs. (18) and (19), which apply only to the mass 60 isotopologue, are treated as known quantities taken from Wolthers et al. (2012). Note that AR^i

includes the attachment rates of both B_1 and B_2 and DR^i includes the detachment rates of both B_1 and B_2.

Because clumped isotope compositions are defined in terms of isotopologues, it is useful to cast Eqs. (17) in terms of isotopologue ratios instead of isotope ratios. It is also useful to have a consistent expression for the oxygen and carbon isotope fractionation factors; rather than cast oxygen isotope compositions relative to water and carbon isotope compositions relative to DIC, we hereafter write the non-equilibrium calcite isotope compositions relative to the carbonate ion for both carbon and oxygen isotopes. This makes for easier comparison between the expressions for carbon and oxygen isotopes and leads to cleaner expressions when we adapt the model for clumped isotopes. Expanding the α's and combining Eqs. (17a) and (17b) leads to:

$$\frac{r^{62}_{xtl}}{3R^{O}_{w}} = \frac{\frac{r^{eq,62}_{xtl}}{3R^{O}_{w}}AR^{60}}{\frac{r^{eq,62}_{xtl}}{3R^{O}_{w}}\left(AR^{60}-DR^{60}\right)(1+\phi)}{\alpha^{f,62}_{xtl-B_1}\frac{r^{eq,62}_{B_1}}{3R^{O}_{w}}+\phi\alpha^{f,62}_{xtl-B_2}\frac{r^{eq,62}_{B_2}}{3R^{O}_{w}}}+DR^{60}}, \tag{20}$$

where the factors of $3R^{O}_{w}$ cancel out. Note that $\alpha^{f,O}_{xtl-B_1} = \alpha^{f,62}_{xtl-B_1}$ because the factor of 3 that relates oxygen isotope ratios to isotopologue ratios in the crystal also shows up in the expressions for DIC species, and cancels out. The molar ratio of any isotopologue with mass i relative to the mass 60 isotopologue can then be given by:

$$r^{i}_{xtl} = \frac{r^{eq,i}_{xtl}AR^{60}}{r^{eq,i}_{xtl}\left(AR^{60}-DR^{60}\right)\frac{AR^{60}}{AR^{i}}+DR^{60}}, \tag{21a}$$

where (see Appendix A.1 for derivation)

$$\frac{AR^{60}}{AR^{i}} = \frac{(1+\phi)}{\alpha^{f,i}_{xtl-B_1}r^{eq,i}_{B_1}+\phi\alpha^{f,i}_{xtl-B_2}r^{eq,i}_{B_2}}, \tag{21b}$$

which states that the non-equilibrium isotopic composition of calcite is a function of the specified equilibrium composition and the relative rates of ion attachment versus detachment of each isotopologue during crystal growth. The new expression for the oxygen isotope composition of calcite is:

$$\alpha^{O}_{xtl-B_1} = \frac{AR^{60}\alpha^{eq,O}_{xtl-B_1}}{\frac{\alpha^{eq,O}_{xtl-B_1}\left(AR^{60}-DR^{60}\right)(1+\phi)}{\alpha^{f,O}_{xtl-B_1}+\phi\alpha^{f,O}_{xtl-B_2}\alpha^{eq,O}_{B_2-B_1}}+DR^{60}} \tag{22}$$

and the analogous expression for the carbon isotope composition of calcite is:

$$\alpha^{C}_{xtl-B_1} = \frac{AR^{60}\alpha^{eq,C}_{xtl-B_1}}{\frac{\alpha^{eq,C}_{xtl-B_1}\left(AR^{60}-DR^{60}\right)(1+\phi)}{\alpha^{f,C}_{xtl-B_1}+\phi\alpha^{f,C}_{xtl-B_2}\alpha^{eq,C}_{B_2-B_1}}+DR^{60}}, \tag{23}$$

where all terms with a superscript 'eq' are treated as knowns (Table 1). The AR^{60} and DR^{60} terms can be calculated using parameter values (attachment/detachment frequencies, kink formation energy, edge work, and speciation on the crystal surface) from the ion-by-ion calcite growth model of Wolthers et al. (2012) (see Tables 2 and 3 in Watkins et al., 2014, for a summary). This leaves the kinetic fractionation factors as the only 'unknown' quantities needed to solve for the isotopic composition of non-equilibrium calcite.

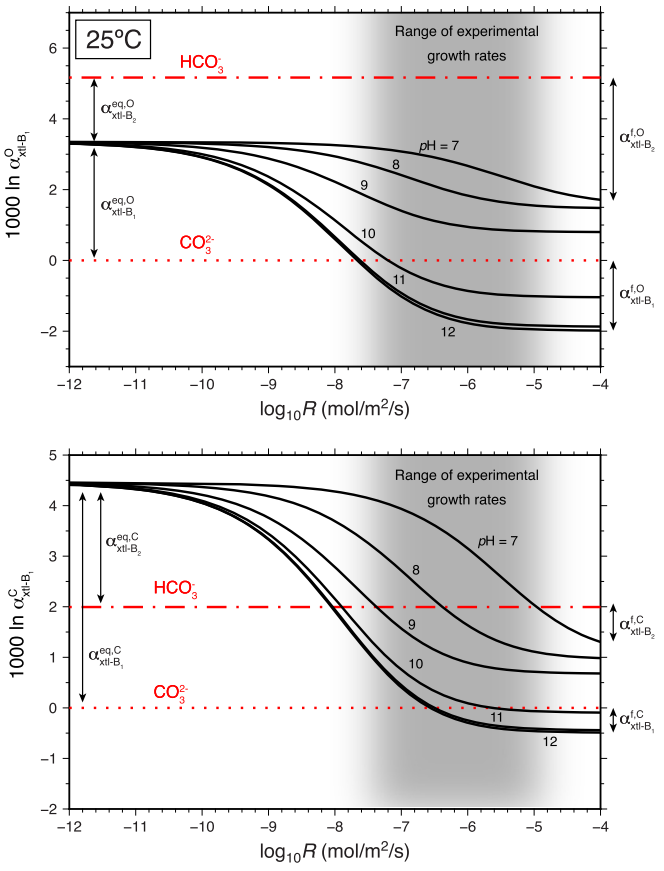

Fig. 2. Modeled stable isotope compositions as a function of growth rate and pH at 25 °C. *Top*: Oxygen isotope systematics. *Bottom*: Carbon isotope systematics. All curves show compositions expressed relative to the stable isotope composition of dissolved CO_3^{2-} following Eqs. (22) and (23). At very low supersaturations (slow growth), the equilibrium composition of calcite is determined by the specified equilibrium fractionation factors. At high growth rates (kinetic limit), the composition of non-equilibrium calcite is determined by the kinetic fractionation factors and the relative proportions of HCO_3^- and CO_3^{2-} participating in calcite growth. For example, at pH = 7, HCO_3^- is the predominant species and the composition of calcite in the fast-growth limit is offset from HCO_3^- by $1000\ln\alpha^{f}_{xtl-B_2}$. Similarly, at pH = 12, CO_3^{2-} is the predominant species and the composition of calcite in the fast-growth limit is offset from CO_3^{2-} by $1000\ln\alpha^{f}_{xtl-B_1}$.

The two functions above are plotted versus the model-derived crystal growth rate (cf. Watkins et al., 2014) in Fig. 2 for arbitrary choices of the kinetic fractionation factors. The equations recover the equilibrium carbon and oxygen isotopic compositions in the limit of extremely slow growth. At fast growth rates, the model-derived isotopic compositions are dictated by the specified kinetic fractionation factors. More specifically, $\alpha^{f}_{xtl-B_1}$ represents a kinetic limit to the degree of isotopic fractionation between calcite and CO_3^{2-} while $\alpha^{f}_{xtl-B_2}$ represents a kinetic limit to the degree of isotopic fractionation between calcite and HCO_3^-. This is most clearly seen at pH values where only one of the two dissolved species is participating in calcite growth. At pH values between 7 and 12, both HCO_3^- and CO_3^{2-} are involved and the isotopic composition of calcite in the kinetic limit reflects the relative contributions of HCO_3^- and CO_3^{2-} (and their respective kinetic fractionation factors) to the isotopic composition of the mineral.

4. Ion-by-ion model for clumped isotopes

As is the case for carbon and oxygen isotopes, each DIC species in aqueous solution has a unique equilibrium clumped isotope composition (Hill et al., 2014). A potentially useful framework for

constructing a process-based model for what governs bond ordering in carbonates is to consider the abundance of mass 63 isotopologues in HCO_3^- and CO_3^{2-} and the extent to which each species contributes mass 63 molecules to the crystal. This is the approach that is followed below. Before we begin, it is important to emphasize that although the isotopic ion-by-ion growth model is constructed on the basis of molecular building blocks of calcite, it does not require that HCO_3^- and CO_3^{2-} be viewed as indestructible molecules throughout the steps involved in ion incorporation into the growing mineral (Watkins et al., 2014).

4.1. Calculating the Δ_{xtl}^{63} of non-equilibrium calcite

4.1.1. Expression for r_{xtl}^{63}

For the doubly-substituted isotopologue, we use Eq. (21) where $i = 63$:

$$r_{xtl}^{63} = \frac{AR^{60} r_{xtl}^{eq,63}}{r_{xtl}^{eq,63}\left(AR^{60} - DR^{60}\right)\dfrac{AR^{60}}{AR^{63}} + DR^{60}}, \tag{24}$$

which states that the non-equilibrium abundance of mass 63 isotopologues in calcite is a function of the specified equilibrium composition and the relative rates of ion attachment versus detachment. As is the case for oxygen and carbon isotopes, the attachment–detachment kinetics for the heavier isotopologues differ slightly from those for the mass 60 isotopologue. The ratio of isotopologue-specific attachment rates is folded into the AR^{60}/AR^{63} term:

$$\frac{AR^{60}}{AR^{63}} = \frac{1+\phi}{\alpha_{xtl-B_1}^{f,63} r_{B_1}^{eq,63} + \phi\alpha_{xtl-B_2}^{f,63} r_{B_2}^{eq,63}}, \tag{25}$$

where

$$r_{B_1}^{eq,63} = r_{B_1*}^{eq,63}\left(\frac{\Delta_{B_1}^{eq,63}}{1000} + 1\right) \tag{26}$$

and

$$r_{B_2}^{eq,63} = r_{B_2*}^{eq,63}\left(\frac{\Delta_{B_2}^{eq,63}}{1000} + 1\right). \tag{27}$$

By substitution we now have

$$r_{xtl}^{63} = \frac{AR^{60} r_{xtl*}^{eq,63}\left(\dfrac{\Delta_{xtl}^{eq,63}}{1000} + 1\right)}{\dfrac{r_{xtl*}^{eq,63}\left(\dfrac{\Delta_{xtl}^{eq,63}}{1000} + 1\right)\left(AR^{60} - DR^{60}\right)(1+\phi)}{\alpha_{xtl-B_1}^{f,63} r_{B_1*}^{eq,63}\left(\dfrac{\Delta_{B_1}^{eq,63}}{1000} + 1\right) + \phi\alpha_{xtl-B_2}^{f,63} r_{B_2*}^{eq,63}\left(\dfrac{\Delta_{B_2}^{eq,63}}{1000} + 1\right)} + DR^{60}}. \tag{28}$$

Values for $\Delta_{B_1}^{eq,63}$, $\Delta_{B_2}^{eq,63}$, $\Delta_{xtl}^{eq,63}$ can be taken from Hill et al. (2014), so all that is needed to obtain a model-derived Δ_{xtl}^{63} are expressions for the stochastic ratios for B_1, B_2, equilibrium calcite and non-equilibrium calcite.

4.1.2. Expressions for the equilibrium stochastic ratios

Computation of the stochastic ratio of mass 63 to mass 60 isotopologues in each of the dissolved species and/or calcite requires knowledge of the $^{18}O/^{16}O$ and $^{13}C/^{12}C$ ratios. Without ^{17}O, there are three indistinguishable $^{13}C^{16}O^{16}O^{18}O$ molecules of mass 63 (the ^{18}O can be in any of the three sites), making the conversion straightforward. The stochastic ratio is

$$r_*^{63} = \frac{3\left[^{13}C\right]\left[^{16}O\right]\left[^{16}O\right]\left[^{18}O\right]}{\left[^{12}C\right]\left[^{16}O\right]\left[^{16}O\right]\left[^{16}O\right]} = 3R^C R^O, \tag{29}$$

which can be calculated for a given T, pH, and growth rate from the output of the ion-by-ion growth model for carbon and oxygen isotopes. The stochastic ratio for each of the equilibrated DIC species and equilibrium calcite can be written in terms of their oxygen and carbon isotopic compositions, which in turn, can be written in terms of the oxygen and carbon isotope compositions of CO_3^{2-} and conventional fractionation factors:

$$r_{B_1*}^{eq,63} = 3R_{B_1}^O R_{B_1}^C \tag{30}$$

$$r_{B_2*}^{eq,63} = 3R_{B_1}^O R_{B_1}^C \alpha_{B_2-B_1}^{eq,O} \alpha_{B_2-B_1}^{eq,C} \tag{31}$$

$$r_{xtl^*}^{eq,63} = 3R_{B_1}^O R_{B_1}^C \alpha_{xtl-B_1}^{eq,O} \alpha_{xtl-B_1}^{eq,C} \tag{32}$$

The equilibrium α's in the above equations are known from experiments (Beck et al., 2005; Zeebe, 2007; Wang et al., 2013) and natural cave calcites (Coplen, 2007; Kluge et al., 2014).

4.1.3. Non-stochastic ratio for non-equilibrium calcite

We can now substitute the equations from the previous section into Eq. (28) to obtain:

$$r_{xtl}^{63} = \frac{AR^{60} 3R_{B_1}^O R_{B_1}^C \alpha_{xtl-B_1}^{eq,O} \alpha_{xtl-B_1}^{eq,C}\left(\dfrac{\Delta_{xtl}^{eq,63}}{1000} + 1\right)}{\dfrac{3R_{B_1}^O R_{B_1}^C \alpha_{xtl-B_1}^{eq,O} \alpha_{xtl-B_1}^{eq,C}\left(\dfrac{\Delta_{xtl}^{eq,63}}{1000} + 1\right)\left(AR^{60} - DR^{60}\right)(1+\phi)}{\alpha_{xtl-B_1}^{f,63} 3R_{B_1}^O R_{B_1}^C\left(\dfrac{\Delta_{B_1}^{eq,63}}{1000} + 1\right) + \phi\alpha_{xtl-B_2}^{f,63} 3R_{B_1}^O R_{B_1}^C \alpha_{B_2-B_1}^{eq,O} \alpha_{B_2-B_1}^{eq,C}\left(\dfrac{\Delta_{B_2}^{eq,63}}{1000} + 1\right)} + DR^{60}}, \tag{33}$$

where $3R_{B_1}^O R_{B_1}^C$ cancels out of the denominator, leaving:

$$r_{xtl}^{63} = \frac{AR^{60} 3R_{B_1}^O R_{B_1}^C \alpha_{xtl-B_1}^{eq,O} \alpha_{xtl-B_1}^{eq,C}\left(\dfrac{\Delta_{xtl}^{eq,63}}{1000} + 1\right)}{\dfrac{\alpha_{xtl-B_1}^{eq,O} \alpha_{xtl-B_1}^{eq,C}\left(\dfrac{\Delta_{xtl}^{eq,63}}{1000} + 1\right)\left(AR^{60} - DR^{60}\right)(1+\phi)}{\alpha_{xtl-B_1}^{f,63}\left(\dfrac{\Delta_{B_1}^{eq,63}}{1000} + 1\right) + \phi\alpha_{xtl-B_2}^{f,63} \alpha_{B_2-B_1}^{eq,O} \alpha_{B_2-B_1}^{eq,C}\left(\dfrac{\Delta_{B_2}^{eq,63}}{1000} + 1\right)} + DR^{60}}. \tag{34}$$

4.1.4. Stochastic ratio for non-equilibrium calcite

The stochastic ratio for non-equilibrium calcite can be obtained by using Eq. (29) and the definitions of conventional fractionation factors to obtain:

$$r_{xtl*}^{63} = 3R_{B_1}^C R_{B_1}^O \alpha_{xtl-B_1}^C \alpha_{xtl-B_1}^O. \tag{35}$$

Further substitution of Eq. (22) and (23) into Eq. (35) leads to:

$$r_{xtl*}^{63} = \frac{3R_{B_1}^O R_{B_1}^C \alpha_{xtl-B_1}^{eq,C} \alpha_{xtl-B_1}^{eq,O}\left(AR^{60}\right)^2}{\left(\dfrac{\alpha_{xtl-B_1}^{eq,C}\left(AR^{60} - DR^{60}\right)(1+\phi)}{\alpha_{xtl-B_1}^{f,C} + \phi\alpha_{xtl-B_2}^{f,C} \alpha_{B_2-B_1}^{eq,C}} + DR^{60}\right)\left(\dfrac{\alpha_{xtl-B_1}^{eq,O}\left(AR^{60} - DR^{60}\right)(1+\phi)}{\alpha_{xtl-B_1}^{f,O} + \phi\alpha_{xtl-B_2}^{f,O} \alpha_{B_2-B_1}^{eq,O}} + DR^{60}\right)}. \tag{36}$$

This general expression links directly, for the first time, the stochastic ratio in calcite to physical quantities that describe the growth of calcite under non-equilibrium conditions. Validation of this expression is provided in Appendix A.2.

4.1.5. Generate final Δ^{63}_{xtl}

We can now combine the non-stochastic ratio (Eq. (34)) and the stochastic ratio (Eq. (36)) to get the final Δ^{63}_{xtl}:

$$\Delta^{63}_{xtl} = 1000\left(\frac{r^{63}_{xtl}}{r^{63}_{xtl*}} - 1\right), \tag{37}$$

where

$$\frac{r^{63}_{xtl}}{r^{63}_{xtl*}} = \frac{\left(\frac{\alpha^{eq,C}_{xtl-B_1}\left(AR^{60} - DR^{60}\right)(1+\phi)}{\alpha^{f,C}_{xtl-B_1} + \phi\alpha^{f,C}_{xtl-B_2}\alpha^{eq,C}_{B_2-B_1}} + DR^{60}\right)\left(\frac{\alpha^{eq,O}_{xtl-B_1}\left(AR^{60} - DR^{60}\right)(1+\phi)}{\alpha^{f,O}_{xtl-B_1} + \phi\alpha^{f,O}_{xtl-B_2}\alpha^{eq,O}_{B_2-B_1}} + DR^{60}\right)\left(\frac{\Delta^{eq,63}_{xtl}}{1000}+1\right)}{AR^{60}\left(DR^{60} + \frac{\alpha^{eq,O}_{xtl-B_1}\alpha^{eq,C}_{xtl-B_1}\left(\frac{\Delta^{eq,63}_{xtl}}{1000}+1\right)\left(AR^{60} - DR^{60}\right)(1+\phi)}{\alpha^{f,63}_{xtl-B_1}\left(\frac{\Delta^{eq,63}_{B_1}}{1000}+1\right) + \phi\alpha^{f,63}_{xtl-B_2}\alpha^{eq,O}_{B_2-B_1}\alpha^{eq,C}_{B_2-B_1}\left(\frac{\Delta^{eq,63}_{B_2}}{1000}+1\right)}\right)}. \tag{38}$$

Most of the symbols in Eq. (38) can be treated as known quantities; if the equilibrium and kinetic fractionation factors for carbon and oxygen isotopes are known or specified, then the only two free parameters are the kinetic fractionation factors for the mass 63 isotopologue. As we show in the next section, however, the kinetic parameters for the mass 63 isotopologue are in fact constrained by the kinetic fractionation factors for the mass 62 and mass 61 isotopologues.

It should be noted that the equilibrium condition is recovered when the attachment rate is equal to the detachment rate. Mathematically, AR → DR, so AR − DR → 0 and AR/DR → 1, leading to:

$$\frac{r^{63}_{xtl}}{r^{63}_{xtl*}} = \frac{\Delta^{eq,63}_{xtl}}{1000} + 1. \tag{39}$$

In the kinetic limit, DR → 0 and AR cancels out, leading to:

$$\frac{r^{63}_{xtl}}{r^{63}_{xtl*}} = \frac{(1+\phi)\left(\alpha^{eq,C}_{B_2-B_1}\alpha^{eq,O}_{B_2-B_1}\alpha^{f,63}_{xtl-B_2}\phi\left(\frac{\Delta^{63}_{B_2}}{1000}+1\right) + \alpha^{f,63}_{xtl-B_1}\left(\frac{\Delta^{63}_{B_1}}{1000}+1\right)\right)}{\left(\alpha^{eq,C}_{B_2-B_1}\alpha^{f,C}_{xtl-B_2}\phi + \alpha^{f,C}_{xtl-B_1}\right)\left(\alpha^{eq,O}_{B_2-B_1}\alpha^{f,O}_{xtl-B_2}\phi + \alpha^{f,O}_{xtl-B_1}\right)}. \tag{40}$$

Although this expression does not lend itself to a simple interpretation, its behavior is remarkably straightforward to interpret once the kinetic fractionation factors for the mass 63 isotopologue are properly constrained.

5. What are the kinetic fractionation factors for clumped isotopes?

The fractionation factors for the mass 63 isotopologue are not independent of the fractionation factors for the mass 62 and 61 isotopologues. To see why this must be the case, we consider here the fractionation factors in the equilibrium limit and then apply the insights gained to the treatment of kinetic fractionation factors.

5.1. Relationship between doubly- and singly-substituted fractionation factors in the equilibrium limit

The equilibrium constant for the clumped isotope exchange reaction (Eq. (1)) is

$$K^{63}_{eq} = \frac{\left[{}^{13}C^{18}O^{16}O^{2-}_2\right]\left[{}^{12}C^{16}O^{2-}_3\right]}{\left[{}^{13}C^{16}O^{2-}_3\right]\left[{}^{12}C^{18}O^{16}O^{2-}_2\right]} = \frac{\left[{}^{63}CO^{2-}_3\right]\left[{}^{60}CO^{2-}_3\right]}{\left[{}^{61}CO^{2-}_3\right]\left[{}^{62}CO^{2-}_3\right]}. \tag{41}$$

Dividing all terms on the right-hand side of Eq. (41) by $^{60}CO^{2-}_3$ we can write the above expression in terms of 'conventional' isotopologue ratios:

$$K^{63}_{eq,xtl} = \frac{\left(\frac{\left[{}^{63}CO^{2-}_3\right]}{\left[{}^{60}CO^{2-}_3\right]}\right)_{xtl}}{\left(\frac{\left[{}^{61}CO^{2-}_3\right]}{\left[{}^{60}CO^{2-}_3\right]}\right)_{xtl}\left(\frac{\left[{}^{62}CO^{2-}_3\right]}{\left[{}^{60}CO^{2-}_3\right]}\right)_{xtl}}, \tag{42}$$

where the denominator now corresponds to the equilibrium carbon isotope composition multiplied by the equilibrium oxygen isotope composition of the crystal. Using the definition of equilibrium fractionation factors between calcite and dissolved CO^{2-}_3, Eq. (42) can be recast as

$$K^{63}_{eq,xtl} = \frac{\alpha^{eq,63}_{xtl-B_1}\left(\frac{\left[{}^{63}CO^{2-}_3\right]}{\left[{}^{60}CO^{2-}_3\right]}\right)_{B_1}}{\alpha^{eq,61}_{xtl-B_1}\left(\frac{\left[{}^{61}CO^{2-}_3\right]}{\left[{}^{60}CO^{2-}_3\right]}\right)_{B_1}\alpha^{eq,62}_{xtl-B_1}\left(\frac{\left[{}^{62}CO^{2-}_3\right]}{\left[{}^{60}CO^{2-}_3\right]}\right)_{B_1}}, \tag{43}$$

which is the same as

$$K^{63}_{eq,xtl} = K^{63}_{eq,B_1}\frac{\alpha^{eq,63}_{xtl-B_1}}{\alpha^{eq,61}_{xtl-B_1}\alpha^{eq,62}_{xtl-B_1}}. \tag{44}$$

Rearranging, we arrive at an expression for $\alpha^{eq,63}_{xtl-B_1}$ as a function of known quantities:

$$\alpha^{eq,63}_{xtl-B_1} = \frac{K^{63}_{eq,xtl}}{K^{63}_{eq,B_1}}\alpha^{eq,61}_{xtl-B_1}\alpha^{eq,62}_{xtl-B_1} \approx \alpha^{eq,61}_{xtl-B_1}\alpha^{eq,62}_{xtl-B_1}. \tag{45}$$

From the definitions of $K^{63}_{eq,xtl}$ (Eq. (42)) and $\Delta^{63}_{eq,xtl}$ (Eq. (39)) we can write

$$K^{63}_{eq,xtl} = \left(\frac{\Delta^{63}_{eq,xtl}}{1000}+1\right), \tag{46}$$

which allows us to recast Eq. (45) in terms of Δ^{63} values:

$$\alpha^{eq,63}_{xtl-B_1} = \underbrace{\left(\frac{\Delta^{63}_{eq,xtl}+1000}{\Delta^{63}_{eq,B_1}+1000}\right)}_{\approx 1+10^{-5}}\alpha^{eq,61}_{xtl-B_1}\alpha^{eq,62}_{xtl-B_1}. \tag{47}$$

A similar expression exists for the equilibrium calcite-B_2 fractionation factor:

$$\alpha^{eq,63}_{xtl-B_2} = \underbrace{\left(\frac{\Delta^{63}_{eq,xtl}+1000}{\Delta^{63}_{eq,B_2}+1000}\right)}_{\approx 1+10^{-5}}\alpha^{eq,61}_{xtl-B_2}\alpha^{eq,62}_{xtl-B_2}. \tag{48}$$

Eqs. (47) and (48) show how the fractionation factor for the mass 63 isotopologue is very nearly equal to the product of the fractionation factors for the mass 61 and mass 62 isotopologues. Physically, this reflects the fact that the ^{18}O in the mass 63 isotopologue should fractionate from ^{16}O in nearly the exact same manner as the ^{18}O in the mass 62 isotopologue. That is, during ion transport to the mineral surface, the oxygen isotopes of the doubly-substituted mass 63 isotopologue will be fractionated by an amount given approximately by $\alpha^{eq,62}_{xtl-B_1}$ while the carbon isotopes will be fractionated by an amount given approximately by $\alpha^{eq,61}_{xtl-B_1}$. The relationship is approximate because secondary isotope effects (e.g., ^{13}C affects the bonding behavior of ^{18}O and vice versa) may create deviations from the approximation. The prefactors in Eqs. (47) and (48), which are nearly equal to unity, are important for ensuring that the equilibrium clumped isotope composition is recovered in the equilibrium (slow growth) limit.

5.2. Relationship between doubly- and singly-substituted fractionation factors in the kinetic limit

Using the expressions for the equilibrium fractionation factors as a guide, we propose the following form for the kinetic fractionation factors:

$$\alpha^{f,63}_{xtl-B_1} = \alpha^{f,61}_{xtl-B_1}\alpha^{f,62}_{xtl-B_1} + \epsilon_{B_1} \tag{49}$$

and

$$\alpha^{f,63}_{xtl-B_2} = \alpha^{f,61}_{xtl-B_2}\alpha^{f,62}_{xtl-B_2} + \epsilon_{B_2}, \tag{50}$$

where the ϵ_{B_1} and ϵ_{B_1} are expected to be small, on the order of 10^{-5}, and could plausibly be positive, negative, or zero. We treat $\epsilon_{B_1} = \epsilon_{B_1} = 0$ as the reference case before demonstrating that even small values of ϵ_{B_1} and ϵ_{B_1} have a large influence on the modeled kinetic clumped isotope effects.

6. Results and discussion

6.1. What is the true equilibrium clumped isotope composition?

The first step in performing calculations based on Eq. (38) is to specify the equilibrium carbon and oxygen isotope composition of calcite relative to dissolved CO_3^{2-} as well as the equilibrium clumped isotope composition of calcite. A conclusion drawn from recent laboratory experiments is that most biogenic and laboratory-grown carbonates form in a regime where their stable isotope compositions are not representative of true equilibrium (Dietzel et al., 2009; Watkins et al., 2013). In natural settings, it is possible for inorganic calcite to grow slowly enough for equilibrium to be achieved, and one such example appears to be inorganic calcite from Devils Hole cave, Nevada, which formed under conditions of very low supersaturation at 33.7 °C (Coplen, 2007). The clumped isotope composition of Devils Hole calcite determined by Kluge et al. (2014) is in agreement with the most recent, experimentally-produced inorganic calibration curve of Zaarur et al. (2013), suggesting that (1) the slowly-grown calcites from Devils Hole are the best natural laboratory for anchoring the true equilibrium composition at their formation temperature of 33.7 °C, and (2) it is possible to obtain near-equilibrium clumped isotope compositions in the laboratory.

However, there are now several conflicting clumped isotope calibration curves that have been proposed, some of which are shown in Fig. 4. The Zaarur et al. (2013) calibration is similar to the Ghosh et al. (2006a) calibration whereas the Hill et al. (2014) calibration is similar to the Dennis and Schrag (2010) and Kluge et al. (2015) calibrations (see Fig. 4 and Hill et al., 2014 for comparisons). The curves for these different calibrations intersect at about 34 °C, such that the Devils Hole cave cannot be used to argue in favor of one calibration over the others. Therefore, until other natural calcites can be identified as having formed under conditions that approach true thermodynamic equilibrium, assumptions must be made regarding the temperature dependence of the equilibrium $\Delta^{47}_{calcite}$. In the absence of available experimental data, calculated temperature dependencies of DIC species and calcite can be used (Hill et al., 2014). The following equations are fits to the calculated data of Hill et al. (2014) between 0 and 100 °C for calcite, CO_3^{2-}, and HCO_3^-:

$$\Delta^{63}_{eq,xtl} = 37.55\frac{1000}{T_K^2} - 0.0296, \tag{51a}$$

$$\Delta^{63}_{eq,B_1} = 36.36\frac{1000}{T_K^2} - 0.0397, \tag{51b}$$

and

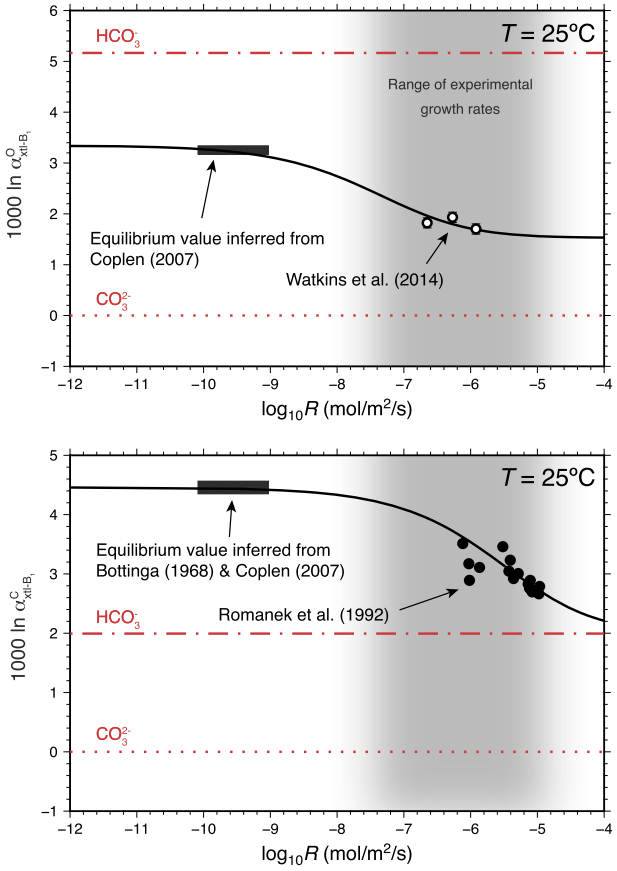

Fig. 3. Experimental constraints on kinetic oxygen and carbon isotope fractionation factors. For both isotopic systems, the equilibrium isotopic composition is inferred from slowly-grown calcites at Devils Hole cave, Nevada (Coplen, 2007). *Top*: Results from experiments at $T = 25$ °C and pH = 8.3 where inorganic calcite was precipitated in the presence of carbonic anhydrase (Watkins et al., 2014). *Bottom*: Results from experiments at $T = 25$ °C and pH = 6.6 to 7.3 where inorganic calcite was precipitated in the presence of a DIC pool with known $\delta^{13}C$ (Romanek et al., 1992). The kinetic fractionation factors used to construct the model curves are $\alpha^{f,O}_{xtl-B_1} = 0.9980$, $\alpha^{f,O}_{xtl-B_2} = 0.9964$, $\alpha^{f,C}_{xtl-B_1} = 1.0000$, and $\alpha^{f,C}_{xtl-B_2} = 1.0000$.

$$\Delta^{63}_{eq,B_2} = 38.35\frac{1000}{T_K^2} - 0.0291. \tag{51c}$$

We use these equations for self-consistency while recognizing that the Hill et al. (2014) results may in fact underestimate the difference between the clumped isotope composition of dissolved HCO_3^- and CO_3^{2-}. The Hill et al. (2014) study predicts $\Delta^{63}_{HCO_3^-} - \Delta^{63}_{CO_3^{2-}} \approx 0.033‰$, which is considerably less than the value of $0.063 \pm 0.006‰$ deduced from recent witherite experiments (Tripati et al., 2015).

6.2. Kinetic fractionation factors

Once the equilibrium fractionation factors are specified, one must then input the kinetic fractionation factors for carbon and oxygen isotopes. For oxygen isotopes, the kinetic fractionation factors have been inferred from the pH-dependence of α^{O}_{xtl-w} measured from calcites precipitated in the presence of an isotopically equilibrated DIC pool (Watkins et al., 2014). For carbon isotopes, the existing data are restricted to pH < 7.8 (Romanek et al., 1992) from which the kinetic fractionation factors are inferred to be close to unity (Fig. 3). Although it is not immediately obvious, the choice of kinetic fractionation factors for oxygen and carbon isotopes is actually not important when it comes to modeling the clumped isotope composition of non-equilibrium calcite because the kinetic

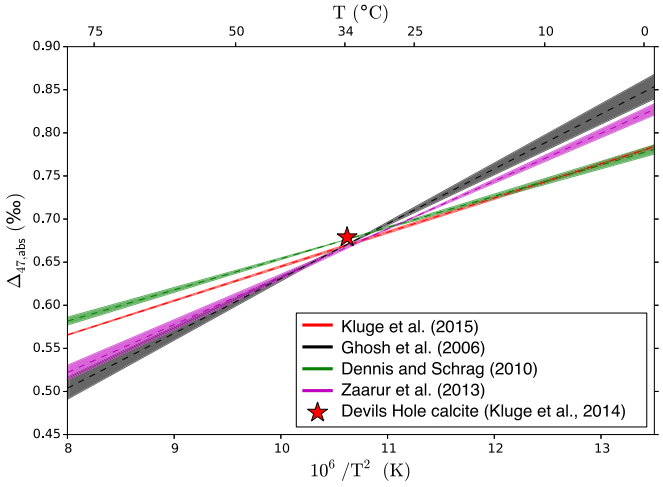

Fig. 4. Four different calibrations of the clumped isotope thermometer with 95% confidence intervals, presented in the absolute reference frame (Dennis et al., 2011) and normalized to a 25 °C acid digestion temperature. The agreement between slowly-grown Devils Hole calcite with the calibration curves has been used to argue that Devils Hole represents the best natural laboratory for measuring the true equilibrium composition (Kluge et al., 2014). Because the curves intersect at the approximate temperature of the Devils Hole samples, however, Devils Hole calcite cannot be used to argue in favor one calibration over the others.

fractionation factor for the mass 63 isotopologue is written as the product of the kinetic fractionation factors for carbon and oxygen isotopes (Eqs. (49) and (50)). An outcome of this relationship is that the results for clumped isotopes have an extremely weak dependence on the input values for the carbon and oxygen kinetic fractionation factors because of how clumped isotope compositions depend upon the carbon and oxygen isotope composition of calcite via the stochastic distribution. For any reasonable range of carbon and oxygen kinetic fractionation factors, the results for clumped isotopes are essentially independent of those factors. As shown in the model outputs presented below, the important parameters dictating the rate- and pH-dependence of kinetic Δ^{63} effects in non-equilibrium calcite are the small ϵ values in Eqs. (49) and (50).

6.3. Model behavior

Although Eq. (38) is a complicated algebraic expression, the behavior that emerges is relatively straightforward to interpret. The modeled rate-dependence of Δ^{63}_{xtl} is presented in Fig. 5 (top) for the reference case where ϵ_{B_1} and ϵ_{B_2} are equal to zero. The curves have a similar to shape to those for oxygen isotopes and carbon isotopes; in the limit of extremely slow growth, the clumped isotope composition is equal to the specified equilibrium composition, and with increasing growth rate, there is an asymptotic approach to a kinetic limit on Δ^{63}_{xtl}. The pH-dependence for both the slow- and fast-growth limits is shown in Fig. 5 (bottom). When the ϵ_{B_1} and ϵ_{B_2} parameters are equal to zero, calcite acquires the clumped isotope composition of DIC in the limit of fast growth. This is analogous to the case for oxygen (or carbon) isotopes where the forward fractionation factors are equal to one.

There is no reason to believe *a priori* that the ϵ_{B_1} and ϵ_{B_2} parameters should be exactly equal to zero based on Eqs. (47)–(50). Fig. 6 shows the pH-dependence at two different (relatively fast) growth rates for additional scenarios where ϵ_{B_1} and $\epsilon_{B_2} \neq 0$. Also shown are the corresponding curves for carbon and oxygen isotopes for arbitrary choices of the kinetic fractionation factors. A positive value of ϵ_{B_1} or ϵ_{B_2} describes an increase in bond ordering at the mineral surface relative to the dissolved species (curves labeled "1"). Conversely, a negative ϵ_{B_1} or ϵ_{B_2} corresponds to a decrease in bond ordering relative to the dissolved species (curves

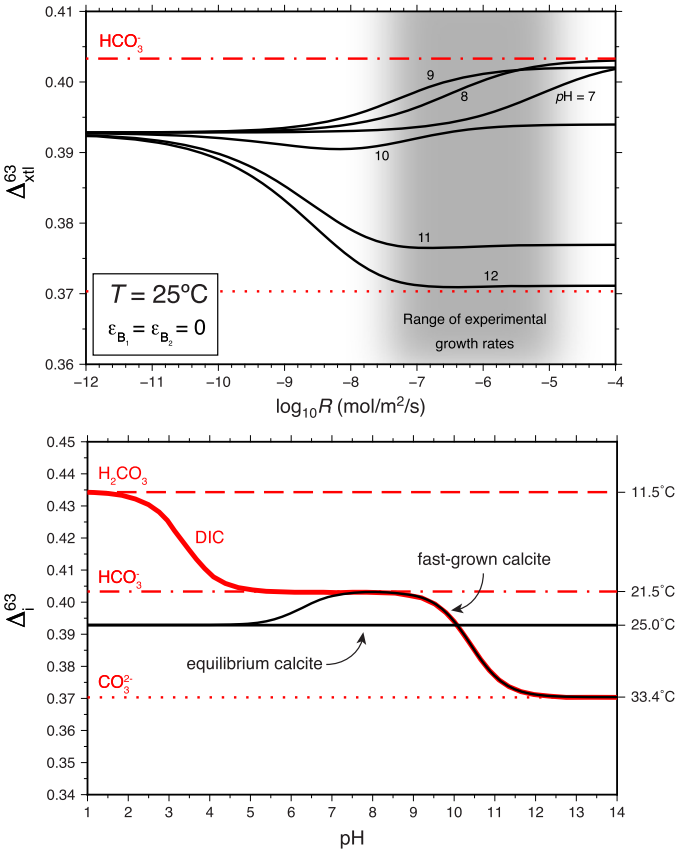

Fig. 5. Modeled rate- and pH-dependence of the clumped isotope composition of non-equilibrium calcite. *Top*: The rate-dependence behaves in much the same way as for carbon and oxygen isotopes (see Fig. 2) insofar as the clumped isotope composition in the fast-growth limit depends on the weighted sum of the clumped isotope compositions of DIC species participating in calcite growth. *Bottom*: The pH-dependence for the two limiting cases of slow growth and fast growth. If the ϵ_{B_1} and $\epsilon_{B_2} = 0$, fast-grown calcite acquires the clumped isotope composition of DIC, regardless of the kinetic fractionation factors for oxygen and carbon isotopes (see text). Although this figure only depicts processes at 25 °C, the second y-axis shows the apparent equivalent temperatures for several chosen Δ^{63}_i values using the Hill et al. (2014) equilibrium calcite calibration. Note that since calcite dissolves at low pH, the model only applies at pH above about 7.

labeled "3"). It is also possible for ϵ_{B_1} and ϵ_{B_2} to have opposite signs but these scenarios are not shown to retain clarity in the figure. As illustrated in these figures, the same general principles that apply to oxygen and carbon isotope discrimination also apply to clumped isotopes: the isotopic composition of non-equilibrium calcite depends on (1) the clumped isotope compositions of HCO_3^- and CO_3^{2-} dissolved in solution, (2) the relative proportions of HCO_3^- and CO_3^{2-} participating in calcite growth, and (3) any increase or decrease in bond ordering that arises during all of the steps involved in ion transport into the mineral lattice, as quantified by the signs and magnitudes of ϵ_{B_1} and ϵ_{B_2}.

6.4. Implications

6.4.1. Inorganic calibrations of the clumped isotope thermometer

It is possible that many of the calcites grown experimentally have isotopic compositions that are offset from the true equilibrium value due to some combination of isotopic disequilibrium among DIC species, isotopic distillation of the DIC pool, pH effects, and growth rate effects. Two recent studies have made progress toward assessing the influence of one or more of these factors. Tang et al. (2014) grew inorganic calcite in an environment where pH and growth rate were controlled. They observed a relatively wide

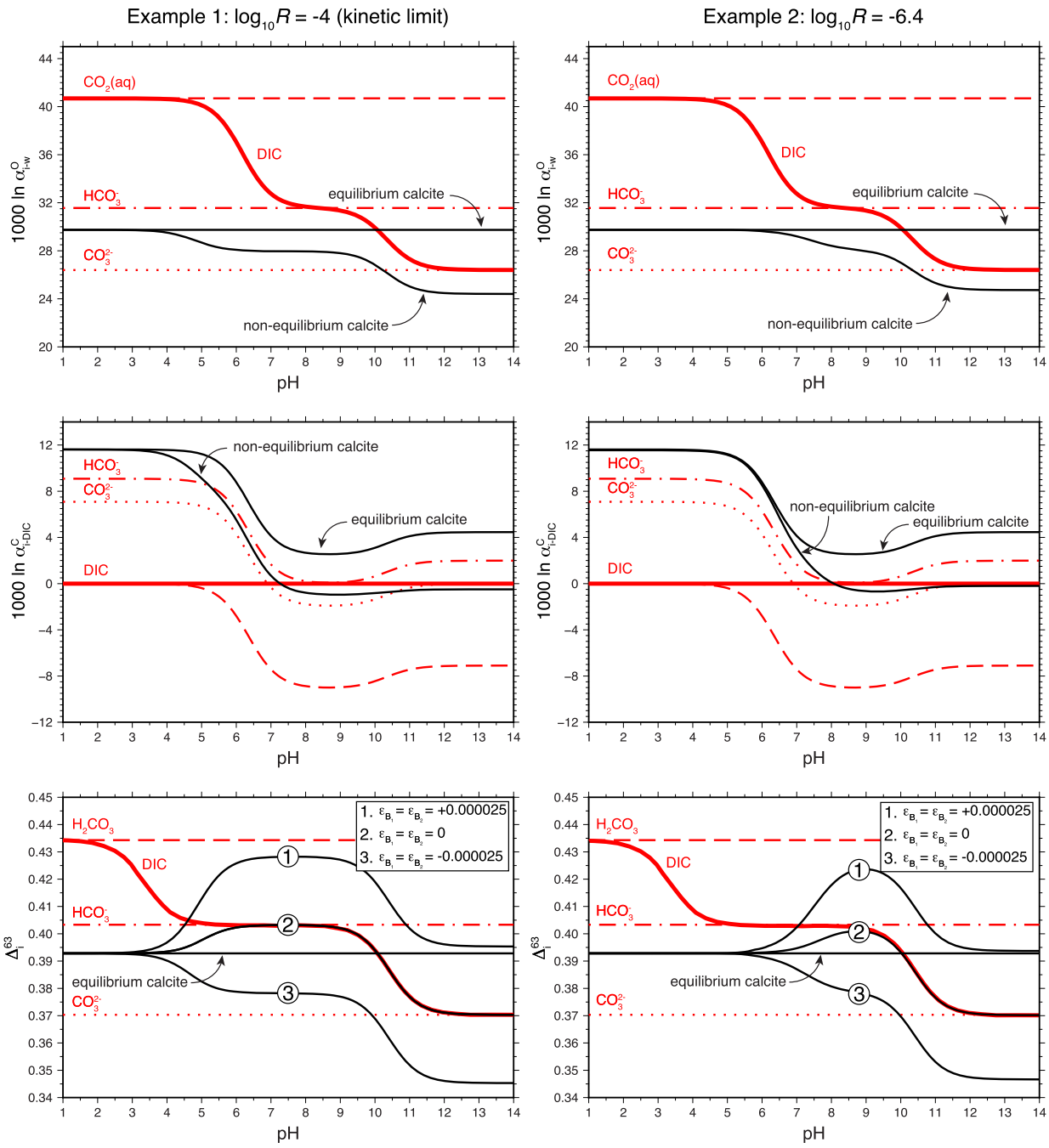

Fig. 6. Modeled pH-dependence of the non-equilibrium isotopic composition of calcite. *Left*: Composition of non-equilibrium calcite in the limit of extremely rapid crystallization. *Right*: Composition of non-equilibrium calcite at $10^{-6.4}$ mol m^{-2} s^{-1}, which is representative of experimentally precipitated calcites (Dietzel et al., 2009; Tang et al., 2014). For carbon and oxygen isotopes, we use the following kinetic fractionation factors for illustrative purposes: $\alpha^{f,O}_{xtl-B_1} = 0.9980$, $\alpha^{f,O}_{xtl-B_2} = 0.9964$, $\alpha^{f,C}_{xtl-B_1} = 0.9995$, $\alpha^{f,C}_{xtl-B_2} = 0.9990$. For clumped isotopes, the carbon and oxygen fractionation factors are arbitrary for reasons discussed in the main text.

range in Δ^{47}_{xtl} at a given temperature of about 0.006‰, comparable to other experimental studies that lacked such controls (e.g., Ghosh et al., 2006a; Dennis and Schrag, 2010; Zaarur et al., 2013; Defliese et al., 2015). This observation, in combination with the fact that the time required to achieve clumped isotope equilibrium among DIC species is about 10 h at 25 °C (cf. Affek, 2013; Clog et al., 2015; Tang et al., 2014), suggests that an out-of-equilibrium DIC pool may be contributing to the scatter in the data from many previous studies in ways that are not well understood. According to our model, the data from Tang et al. (2014) would be unable to resolve the expected pH- or rate-dependence on Δ^{47}_{xtl}, consistent with their findings. More recently, Tripati et al. (2015) grew calcite in the presence of the enzyme carbonic anhydrase, which promotes isotopic equilibration among DIC species, but since their experiments controlled neither pH nor growth rate, these results are also not directly comparable to model outputs. We anticipate that ongoing experiments designed to measure the pH- and rate-dependence of Δ^{47} of calcite grown from an isotopically equilibrated DIC pool will be useful for constraining the kinetic fractionation factors and interpreting data from previous inorganic calcite precipitation experiments. Meanwhile, the calculations presented thus far offer a semi-quantitative explanation for

why the various calibrations of the clumped isotope thermometer are broadly similar despite the lack of experimental control of pH, growth rate, and the isotopic composition of the DIC pool; surface reaction controlled kinetic effects restrict Δ^{63}_{xtl} to a range of values between Δ^{63}_{eq,HCO_3^-} and Δ^{63}_{eq,CO_3^-} (assuming ϵ_{B_1} and $\epsilon_{B_2} = 0$) that differ from the $\Delta^{63}_{eq,xtl}$ by only a few 0.001‰. Larger differences, where observed, would require that ϵ_{B_1} and $\epsilon_{B_2} \neq 0$, which could be a manifestation of isotopic disequilibrium among DIC species, as discussed further below.

6.4.2. Kinetic effects in forams, coccoliths, and deep-sea corals

An observation that has warranted considerable discussion is that planktic foraminifera, coccoliths, benthic foraminifera, and deep-sea corals exhibit large 'vital effects' with respect to $\delta^{13}C$ and $\delta^{18}O$ but little to no vital effect with respect to clumped isotopes (Tripati et al., 2010; Thiagarajan et al., 2011). A number of hypotheses have been considered to explain this observation, including isotopic mixing of samples with different bulk isotopic compositions, incomplete exchange of carbon and oxygen isotopes among DIC species, diffusive transport of DIC species, and direct inheritance of isotopes from bulk DIC (Tripati et al., 2010; Thiagarajan et al., 2011). The latter hypothesis has perhaps received the most support since it can explain (a) why so many different types of carbonates fall on the same Δ^{63} versus T calibration line (Tripati et al., 2010; Affek, 2012; Henkes et al., 2013; Hill et al., 2014), (b) why there is no evidence for species-specific offsets in Δ^{47}_{xtl}, and (c) why $\delta^{13}C$ and $\delta^{18}O$ are more sensitive to pH than Δ^{47}_{xtl}. While this hypothesis may be approximately correct, there are clear instances where carbon and oxygen isotopes in carbonates are offset from the isotopic composition of DIC (Spero et al., 1997; Watkins et al., 2014), which precludes the conceptual model wherein carbonates quantitatively precipitate DIC from a finite reservoir near the site of calcification (Tripati et al., 2010). Our calculations show that quantitative precipitation is not required for a carbonate mineral to have the same clumped isotope composition as that of DIC. Instead, we propose that carbonate minerals may acquire a clumped isotope composition similar to that of DIC as a consequence of mass balance and the fact that clumped isotope compositions are calculated relative to a stochastic distribution based on the actual $\delta^{13}C$ and $\delta^{18}O$ values.

6.4.3. Kinetic effects in surface corals

The above conclusion does not directly address why some mollusks and brachiopods, surface corals, and speleothems are displaced from the main calibration line shared by other types of carbonates (Daëron et al., 2011; Saenger et al., 2012; Henkes et al., 2013; Eiler et al., 2014). Focusing on surface corals, for which pH and growth rate are known (Saenger et al., 2012), Fig. 7 shows the difference between the measured clumped isotope composition (Δ^{47}_{meas}) and the expected clumped isotope composition (Δ^{47}_{Hill}). Here, the calculated Δ^{63}_{xtl} were converted to Δ^{47}_{xtl} values using an AFF of 0.28 (acid digestion at 25 °C; Tripati et al., 2015) for the comparison to experimental data. The observation that has been made previously is that surface corals are shifted systematically to higher Δ^{47} values, and therefore lower apparent temperatures, than would be expected from several calibrations of the Δ^{47}–temperature relationship (Saenger et al., 2012; Eiler et al., 2014). The current explanation for this shift is that hydration of excess CO_2 near the calcification site leads to a higher-than-equilibrium Δ^{47} of HCO_3^- which is then inherited by the organism. This conceptual model is quantified by the best-fit ϵ values being greater than 0, which means that the HCO_3^- molecules (and also perhaps the CO_3^{2-}) adsorbed on the mineral surface are less isotopically scrambled than their counterparts in the bulk solution. The ion-by-ion model cannot distinguish whether a positive

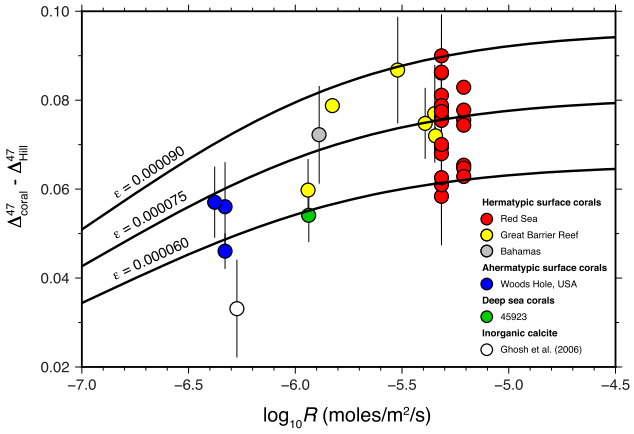

Fig. 7. Measured versus modeled oxygen and clumped isotope compositions of coral calcites from Saenger et al. (2012). The surface corals are displaced to higher Δ^{47}_{xtl} values (or lower apparent temperatures) than expected based on numerous calibrations of the clumped isotope thermometer (cf. Eiler et al., 2014). These deviations can be fit with positive ϵ_{B_1} and ϵ_{B_2} values, which represent a net increase in bond ordering within dissolved HCO_3^- and CO_3^{2-} as a result of all transport processes, including possible disequilibrium among DIC species, that ultimately lead to ion incorporation into the mineral.

ϵ is due to processes near the mineral surface such as desolvation, or whether it reflects an elevated Δ^{47} of HCO_3^- due to kinetics of (de-)hydroxylation and (de-)hydration reactions in the bulk solution. Like the kinetic fractionation factors for carbon and oxygen isotopes, the ϵ parameters are macroscopic in the sense that their values describe the net result of all processes contributing to mass fractionation during isotope exchange and mass transport to the growing mineral, including bond reordering at the mineral–solution interface (Tripati et al., 2015).

7. Summary

We modified an existing ion-by-ion calcite growth model, which describes steady-state calcite growth through the attachment-detachment of Ca^{2+}, HCO_3^- and CO_3^{2-} ions to the crystal surface, to include the isotopologues of HCO_3^- and CO_3^{2-}. The reference scenario for the model is calcite precipitation from an equilibrated DIC pool, wherein the isotopic compositions of dissolved HCO_3^- and CO_3^{2-} are treated as known quantities. Carbon and oxygen isotopic fractionation between calcite and aqueous solution arises through the isotopologue-specific attachment and detachment rates. The clumped isotope composition of calcite is calculated from the carbon and oxygen isotope composition and the mass fractionation behavior of the doubly-substituted isotopologue. Although the model is constructed on the basis of molecular building blocks of calcite, this does not imply that the isotopologues of HCO_3^- and CO_3^{2-} are indestructible molecules that maintain their isotopic identity throughout the steps (e.g., aqueous diffusion, ion desolvation, surface diffusion and isotope exchange/reordering reactions at the aqueous–mineral interface) involved in ion incorporation into the growing mineral. The equations represent a self-consistent framework for calculating the carbon, oxygen, and clumped isotope composition of calcite as a function of temperature, crystal growth rate, and solution pH. The derivations and several example outputs presented herein lead to the following key points:

1. The equilibrium fractionation factor for the mass 63 isotopologue can be written as a function of the equilibrium fractionation factors for the mass 62 and mass 61 isotopologues.
2. We propose that the kinetic fractionation factor for the mass 63 isotopologue is equal to the product of the kinetic fraction-

ation factors for the mass 62 and mass 61 isotopologues plus or minus some small deviation, denoted with the symbol ϵ, that is on the order of 10^{-5}.

3. The ϵ parameters describe the extent to which the clumped isotope composition of HCO_3^- and CO_3^{2-} become scrambled or unscrambled during the many steps involved in ion transport to and from the mineral surface. Like the kinetic fractionation factors for oxygen and carbon isotopes, the ϵ parameters are macro-scale parameters that describe the net result of all processes contributing to isotopic fractionation or re-ordering.
4. If the ϵ parameters are equal to zero, the clumped isotope composition of a rapidly-grown carbonate mineral is nearly equal to that of DIC. This may or may not be a common situation. Nevertheless, at the normal pH of seawater, the clumped isotope composition of DIC and equilibrium calcite differ by only 0.01‰. Further, calcites grown at typical growth rates will have a clumped isotope composition between that of rapidly-grown carbonates and equilibrium calcite. This result offers a quantitative rationalization for how foraminifera, coccoliths, and deep sea corals can have near-equilibrium clumped isotope compositions but far-from-equilibrium carbon and oxygen isotope compositions (Tripati et al., 2010; Thiagarajan et al., 2011). It may also help explain why so many different organisms (including those that precipitate aragonite instead of calcite) fall on the same clumped isotope–temperature curve(s).
5. In cases where the ϵ parameters are non-zero, the clumped isotope composition of a rapidly-grown carbonate mineral may deviate significantly from that of DIC. Such deviations may be the simple result of an unequilibrated DIC pool, but it is also conceivable that the ϵ parameters could be non-zero due to processes involved in the transport of HCO_3^- and CO_3^{2-} to and from the mineral surface; i.e., surface reaction-controlled kinetic effects such as those described by the Tripati et al. (2015) conceptual model.
6. It is possible to match the rate-dependence observed in surface corals with positive ϵ parameters. This result does not conflict with previous proposals that kinetic clumped isotope effects in surface corals may be due to rapid hydration of excess CO_2 (Saenger et al., 2012; Eiler et al., 2014).
7. For the model curves presented herein, we have assumed that the kinetic fractionation factors for carbon, oxygen, and clumped isotopes do not depend temperature or other factors such as pH or solution composition. This crude assumption may need to be relaxed if warranted by new experimental data.
8. A particularly useful set of experiments for comparison to previous inorganic calcite calibrations would involve monitoring the pH and growth rate, using a water buffered system with respect to oxygen isotopes, ensuring there is no isotopic distillation of the DIC pool, and ensuring that equilibrium among DIC species is at least approximately maintained during calcite growth.
9. While the model is built upon an existing framework that is specific to the mineral calcite, the steps involved in adapting the model for clumped isotopes should be useful to future developments of quantitative descriptions of non-equilibrium clumped isotope effects in other systems.

Acknowledgements

Mathieu Daeron's online wiki and responses to inquiries on clumped isotopes were very helpful. Section 5.1 benefited from a conversation with D. Stolper at the 2014 AGU conference. We gratefully acknowledge the constructive reviews by Cedric John and Daniel Stolper. This research was supported by the University of Oregon through startup funds to JMW and by the U.S. Department of Energy, Office of Basic Energy Sciences, Division of Chemical, Biological and Geological Sciences through Lawrence Berkeley National Laboratory under contract No. DE-AC02-05CH11231.

Appendix A

A.1. Derivation of the AR^{60}/AR^i expression

The attachment–detachment kinetics for the higher mass isotopologues differ slightly from those for the mass 60 isotopologue. The ratio of isotopologue-specific attachment frequencies can be used to define two kinetic (forward) fractionation factors, one for B_1 and one for B_2 as (see Eqs. 16a and 16b in Watkins et al., 2014):

$$\alpha^{f,i}_{xtl-B_1} = \frac{k^i_{B_1}}{k^{60}_{B_1}}, \tag{A.1}$$

and

$$\alpha^{f,i}_{xtl-B_2} = \frac{k^i_{B_2}}{k^{60}_{B_2}}. \tag{A.2}$$

We can then start with the expression for the attachment rates of each isotopologue:

$$\frac{AR^{60}}{AR^i} = \frac{k_{B_1^{60}}[B_1^{60}]P_A + k_{B_2^{60}}[B_2^{60}]P_A}{k_{B_1^i}[B_1^i]P_A + k_{B_2^i}[B_2^i]P_A}. \tag{A.3}$$

Expanding the denominator we can write

$$\frac{AR^{60}}{AR^i} = \frac{k_{B_1^{60}}[B_1^{60}]P_A + k_{B_2^{60}}[B_2^{60}]P_A}{\alpha^{f,i}_{xtl-B_1}k_{B_1^{60}}[B_1^{60}]r^{eq,i}_{B_1}P_A + \alpha^{f,i}_{xtl-B_2}k_{B_2^{60}}[B_2^{60}]r^{eq,i}_{B_2}P_A}. \tag{A.4}$$

From the Wolthers et al. (2012) model, we use the following relationships:

$$k_{B_1^{60}} = k_{B_2^{60}} \tag{A.5}$$

and

$$\left[B_2^{60}\right] = \phi\left[B_1^{60}\right], \tag{A.6}$$

which leads to

$$\frac{AR^{60}}{AR^i} = \frac{(1+\phi)}{\alpha^{f,i}_{xtl-B_1}r^{eq,i}_{B_1} + \phi\alpha^{f,i}_{xtl-B_2}r^{eq,i}_{B_2}}. \tag{A.7}$$

A.2. Example calculation of the stochastic ratio

A.2.1. Process-based stochastic ratio

For simplicity we continue to assume that there is no ^{17}O. From Eq. (36) we can compute the stochastic ratio using parameter values provided in Table A.1 for $T = 25\,^\circ C$, pH = 8.3 and $\Omega = 7.4$. This yields $r^{63}_{xtl^*} = 7.158820732177469 \times 10^{-5}$ (first two columns of Table A.1).

A.2.2. Non-process-based stochastic ratio

With knowledge of the carbon and oxygen isotope composition of the crystal one can calculate the molar abundances (denoted with the symbol C) of isotopes and isotopologues (last three columns of Table A.1). For the parameters listed ($T = 25\,^\circ C$, pH = 8.3 and $\Omega = 7.4$), the isotopic composition of non-equilibrium calcite is $^{13}C/^{12}C = 0.011222843743774$ and $^{18}O/^{16}O = 0.006378793909653$. Using this as an input and following the

Table A.1
Values used for the example calculation of the stochastic ratio from the ion-by-ion model using Eq. (36). The AR^{60}, DR^{60}, and ϕ parameters correspond to $T = 25\,^{\circ}C$, pH = 8.3 and $\Omega = 7.4$. For these calculations, we use $r_w = 0.0020672$ and $r_{DIC} = 0.0112372$, which represent the oxygen and carbon isotopic composition of Pee Dee Belemnite.

Ion-by-ion model		Canonical approach		
Parameter	Value	Isotope/isotopologue	Mass	Mole fraction
$r^{61}_{B_1}$	0.011216144632026	C_{12}	12	0.988901710623719
$r^{62}_{B_1}$	0.002122496022646	C_{13}	13	0.011098289376281
AR^{60}	14.031689198469467	C_{16}	16	0.997878246772305
DR^{60}	1.904996407891161	C_{18}	18	0.002121753227695
$\alpha^{eq,C}_{xtl-B_1}$	1.004469000100333	$C_{2666} = C_{12}C_{16}C_{16}C_{16}$	60	0.982620440610989
$\alpha^{eq,O}_{xtl-B_1}$	1.003354613133830	$C_{2668} = C_{12}C_{16}C_{16}C_{18} \cdot 3$	62	0.006267933282070
$\alpha^{f,C}_{xtl-B_1}$	1.0000	$C_{2688} = C_{12}C_{16}C_{18}C_{18} \cdot 3$	64	$1.332728488192658 \times 10^{-5}$
$\alpha^{f,C}_{xtl-B_2}$	0.9980	$C_{2888} = C_{12}C_{18}C_{18}C_{18}$	66	$9.445778181893845 \times 10^{-9}$
$\alpha^{f,O}_{xtl-B_1}$	0.9980	$C_{3666} = C_{13}C_{16}C_{16}C_{16}$	61	0.011027795664416
$\alpha^{f,O}_{xtl-B_2}$	0.9964	$C_{3668} = C_{13}C_{16}C_{16}C_{18} \cdot 3$	63	$7.034403582107305 \times 10^{-5}$
$\alpha^{eq,C}_{B_2-B_1}$	1.001995685541594	$C_{3688} = C_{13}C_{16}C_{18}C_{18} \cdot 3$	65	$1.495700357586258 \times 10^{-7}$
$\alpha^{eq,O}_{B_2-B_1}$	1.005179546014960	$C_{3888} = C_{13}C_{18}C_{18}C_{18}$	67	$1.060084925737459 \times 10^{-10}$
ϕ	$1.070823878831513 \times 10^{2}$	–	–	–
$r^{63}_{xtl^*}$	$7.158820732177469 \times 10^{-5}$	$r^{63}_{xtl^*}$		$7.158820732177469 \times 10^{-5}$

canonical approach for calculating the stochastic distribution, we get $r^{63}_{xtl^*} = 7.158820732177469 \times 10^{-5}$, in perfect agreement with the value calculation from Eq. (36). This example calculation is intended to instill confidence in the expressions derived herein for the clumped isotope composition of calcite.

References

Affek, H., 2013. Clumped isotopic equilibrium and the rate of isotope exchange between CO_2 and water. Am. J. Sci. 313, 309–325.

Affek, H.P., 2012. Clumped isotope paleothermometry: principles, applications, and challenges. Reconstructing Earth's Deep-Time Climate – The State of the Art in 2012. Paleontol. Soc. Pap. 18, 101–104.

Affek, H.P., Bar-Matthews, M., Ayalon, A., Matthews, A., Eiler, J.M., 2008. Glacial/interglacial temperature variations in Soreq cave speleothems as recorded by 'clumped isotope' thermometry. Geochim. Cosmochim. Acta 72 (22), 5351–5360.

Beck, W., Grossman, E., Morse, J., 2005. Experimental studies of oxygen isotope fractionation in the carbonic acid system at 15, 25, and 40 °C. Geochim. Cosmochim. Acta 69 (14), 3493–3503.

Bottinga, Y., 1968. Calculation of fractionation factors for carbon and oxygen isotopic exchange in the system calcite–carbon dioxide–water. J. Phys. Chem. 72 (3), 800–808.

Came, R.E., Eiler, J.M., Veizer, J., Azmy, K., Brand, U., Weidman, C.R., 2007. Coupling of surface temperatures and atmospheric CO_2 concentrations during the Palaeozoic era. Nature 449 (7159), 198–201.

Clog, M., Stolper, D., Eiler, J.M., 2015. Kinetics of CO_2(g)–H_2O isotopic exchange, including mass 47 isotopologues. Chem. Geol. 395, 1–10.

Coplen, T., 2007. Calibration of the calcite–water oxygen–isotope geothermometer at Devils Hole, Nevada, a natural laboratory. Geochim. Cosmochim. Acta 71 (16), 3948–3957.

Daëron, M., Guo, W., Eiler, J., Genty, D., Blamart, D., Boch, R., Drysdale, R., Maire, R., Wainer, K., Zanchetta, G., 2011. ^{13}C–^{18}O clumping in speleothems: observations from natural caves and precipitation experiments. Geochim. Cosmochim. Acta 75 (12), 3303–3317.

Defliese, W.F., Hren, M.T., Lohmann, K.C., 2015. Compositional and temperature effects of phosphoric acid fractionation on Δ_{47} analysis and implications for discrepant calibrations. Chem. Geol. 396, 51–60.

Dennis, K., Schrag, D., 2010. Clumped isotope thermometry of carbonatites as an indicator of diagenetic alteration. Geochim. Cosmochim. Acta 74 (14), 4110–4122.

Dennis, K.J., Affek, H.P., Passey, B.H., Schrag, D.P., Eiler, J.M., 2011. Defining an absolute reference frame for 'clumped' isotope studies of CO_2. Geochim. Cosmochim. Acta 75 (22), 7117–7131.

Dietzel, M., Tang, J., Leis, A., Köhler, S., 2009. Oxygen isotopic fractionation during inorganic calcite precipitation: effects of temperature, precipitation rate and pH. Chem. Geol. 268 (1), 107–115.

Eagle, R.A., Tütken, T., Martin, T.S., Tripati, A.K., Fricke, H.C., Connely, M., Cifelli, R.L., Eiler, J.M., 2011. Dinosaur body temperatures determined from isotopic (^{13}C–^{18}O) ordering in fossil biominerals. Science 333 (6041), 443–445.

Eiler, J.M., Bergquist, B., Bourg, I., Cartigny, P., Farquhar, J., Gagnon, A., Guo, W., Halevy, I., Hofmann, A., Larson, T.E., et al., 2014. Frontiers of stable isotope geoscience. Chem. Geol. 372, 119–143.

Eiler, J.M., Schauble, E., 2004. $^{18}O^{13}C^{16}O$ in Earth's atmosphere. Geochim. Cosmochim. Acta 68 (23), 4767–4777.

Ghosh, P., Adkins, J., Affek, H., Balta, B., Guo, W., Schauble, E., Schrag, D., Eiler, J., 2006a. ^{13}C–^{18}O bonds in carbonate minerals: a new kind of paleothermometer. Geochim. Cosmochim. Acta 70 (6), 1439–1456.

Ghosh, P., Garzione, C.N., Eiler, J.M., 2006b. Rapid uplift of the Altiplano revealed through ^{13}C–^{18}O bonds in paleosol carbonates. Science 311 (5760), 511–515.

Guo, W., 2009. Carbonate clumped isotope thermometry: application to carbonaceous chondrites and effects of kinetic isotope fractionation. Ph.D. thesis. California Institute of Technology.

Guo, W., Mosenfelder, J.L., Goddard, W.A., Eiler, J.M., 2009. Isotopic fractionations associated with phosphoric acid digestion of carbonate minerals: insights from first-principles theoretical modeling and clumped isotope measurements. Geochim. Cosmochim. Acta 73 (24), 7203–7225.

Henkes, G.A., Passey, B.H., Wanamaker Jr., A.D., Grossman, E.L., Ambrose Jr., W.G., Carroll, M.L., 2013. Carbonate clumped isotope compositions of modern marine mollusk and brachiopod shells. Geochim. Cosmochim. Acta 106, 307–325.

Hill, P.S., Tripati, A.K., Schauble, E.A., 2014. Theoretical constraints on the effects of pH, salinity, and temperature on clumped isotope signatures of dissolved inorganic carbon species and precipitating carbonate minerals. Geochim. Cosmochim. Acta 125, 610–652.

Kluge, T., Affek, H.P., Dublyansky, Y., Spötl, C., 2014. Devils Hole paleotemperatures and implications for oxygen isotope equilibrium fractionation. Earth Planet. Sci. Lett. 400, 251–260.

Kluge, T., John, C.M., Jourdan, A.-L., Davis, S., Crawshaw, J., 2015. Laboratory calibration of the calcium carbonate clumped isotope thermometer in the 25–250 °C temperature range. Geochim. Cosmochim. Acta 157, 213–227.

Mook, W., 1986. ^{13}C in atmospheric CO_2. Neth. J. Sea Res. 20 (2–3).

Mook, W., Bommerson, J., Staverman, W., 1974. Carbon isotope fractionation between dissolved bicarbonate and gaseous carbon dioxide. Earth Planet. Sci. Lett. 22.

Romanek, C.S., Grossman, E.L., Morse, J.W., 1992. Carbon isotopic fractionation in synthetic aragonite and calcite: effects of temperature and precipitation rate. Geochim. Cosmochim. Acta 56 (1), 419–430.

Saenger, C., Affek, H.P., Felis, T., Thiagarajan, N., Lough, J.M., Holcomb, M., 2012. Carbonate clumped isotope variability in shallow water corals: temperature dependence and growth-related vital effects. Geochim. Cosmochim. Acta 99, 224–242.

Schauble, E.A., Ghosh, P., Eiler, J.M., 2006. Preferential formation of ^{13}C–^{18}O bonds in carbonate minerals, estimated using first-principles lattice dynamics. Geochim. Cosmochim. Acta 70 (10), 2510–2529.

Spero, H.J., Bijma, J., Lea, D.W., Bemis, B.E., 1997. Effect of seawater carbonate concentration on foraminiferal carbon and oxygen isotopes. Nature 390 (6659), 497–500.

Stolper, D., Lawson, M., Davis, C., Ferreira, A., Neto, E.S., Ellis, G., Lewan, M., Martini, A., Tang, Y., Schoell, M., et al., 2014. Formation temperatures of thermogenic and biogenic methane. Science 344 (6191), 1500–1503.

Stolper, D., Martini, A., Clog, M., Douglas, P., Shusta, S., Valentine, D., Sessions, A., Eiler, J., 2015. Distinguishing and understanding thermogenic and biogenic

sources of methane using multiply substituted isotopologues. Geochim. Cosmochim. Acta 161, 219–247.
Tang, J., Dietzel, M., Fernandez, A., Tripati, A., Rosenheim, B., 2014. Evaluation of kinetic effects on clumped isotope fractionation (Δ_{47}) during inorganic calcite precipitation. Geochim. Cosmochim. Acta 134, 120–136.
Thiagarajan, N., Adkins, J., Eiler, J., 2011. Carbonate clumped isotope thermometry of deep-sea corals and implications for vital effects. Geochim. Cosmochim. Acta 75 (16), 4416–4425.
Tripati, A.K., Eagle, R.A., Thiagarajan, N., Gagnon, A.C., Bauch, H., Halloran, P.R., Eiler, J.M., 2010. ^{13}C–^{18}O isotope signatures and 'clumped isotope' thermometry in foraminifera and coccoliths. Geochim. Cosmochim. Acta 74 (20), 5697–5717.
Tripati, A.K., Hill, P.S., Eagle, R.A., Mosenfelder, J.L., Tang, J., Schauble, E.A., Eiler, J.M., Zeebe, R.E., Uchikawa, J., Coplen, T.B., et al., 2015. Beyond temperature: clumped isotope signatures in dissolved inorganic carbon species and the influence of solution chemistry on carbonate mineral composition. Geochim. Cosmochim. Acta 166, 344–371.
Turner, J.V., 1982. Kinetic fractionation of carbon-13 during calcium carbonate precipitation. Geochim. Cosmochim. Acta 46 (7), 1183–1191.
Usdowski, E., Hoefs, J., 1993. Oxygen isotope exchange between carbonic acid, bicarbonate, carbonate, and water: a re-examination of the data of Mccrea (1950) and an expression for the overall partitioning of oxygen isotopes between the carbonate species and water. Geochim. Cosmochim. Acta 57 (15), 3815–3818.
Vogel, J., Grootes, P., Mook, W., 1970. Isotopic fractionation between gaseous and dissolved carbon dioxide. Z. Phys. 230.
Wacker, U., Fiebig, J., Schoene, B.R., 2013. Clumped isotope analysis of carbonates: comparison of two different acid digestion techniques. Rapid Commun. Mass Spectrom. 27 (14), 1631–1642.
Wang, D.T., Gruen, D.S., Lollar, B.S., Hinrichs, K.-U., Stewart, L.C., Holden, J.F., Hristov, A.N., Pohlman, J.W., Morrill, P.L., Könneke, M., et al., 2015. Nonequilibrium clumped isotope signals in microbial methane. Science 348 (6233), 428–431.
Wang, Z., Gaetani, G., Liu, C., Cohen, A., 2013. Oxygen isotope fractionation between aragonite and seawater: developing a novel kinetic oxygen isotope fractionation model. Geochim. Cosmochim. Acta 117, 232–251.
Wang, Z., Schauble, E.A., Eiler, J.M., 2004. Equilibrium thermodynamics of multiply substituted isotopologues of molecular gases. Geochim. Cosmochim. Acta 68 (23), 4779–4797.
Watkins, J.M., Hunt, J.D., Ryerson, F.J., DePaolo, D.J., 2014. The influence of temperature, pH, and growth rate on the $\delta^{18}O$ composition of inorganically precipitated calcite. Earth Planet. Sci. Lett. 404, 332–343.
Watkins, J.M., Nielsen, L.C., Ryerson, F.J., DePaolo, D.J., 2013. The influence of kinetics on the oxygen isotope composition of calcium carbonate. Earth Planet. Sci. Lett. 375, 349–360.
Wolthers, M., Nehrke, G., Gustafsson, J., Van Cappellen, P., 2012. Calcite growth kinetics: modeling the effect of solution stoichiometry. Geochim. Cosmochim. Acta 77, 121–134.
Yeung, L.Y., Ash, J.L., Young, E.D., 2015. Biological signatures in clumped isotopes of O_2. Science 348 (6233), 431–434.
Zaarur, S., Affek, H.P., Brandon, M.T., 2013. A revised calibration of the clumped isotope thermometer. Earth Planet. Sci. Lett. 382, 47–57.
Zeebe, R., 2007. An expression for the overall oxygen isotope fractionation between the sum of dissolved inorganic carbon and water. Geochem. Geophys. Geosyst. 8 (9), Q09002.
Zeebe, R., Wolf-Gladrow, D., 2001. CO_2 in Seawater: Equilibrium, Kinetics, Isotopes, vol. 65. Elsevier Science Limited.